GEOPHYSICS

A national-scale assessment of land subsidence in China's major cities

Zurui Ao[1]†, Xiaomei Hu[2,3]†, Shengli Tao[2,3]*†, Xie Hu[4,3], Guoquan Wang[5], Mingjia Li[6], Fang Wang[7], Litang Hu[8], Xiuyu Liang[9], Jingfeng Xiao[9], Asadilla Yusup[2,3], Wenhua Qi[2,3], Qinwei Ran[2,3], Jiayi Fang[11,12], Jinfeng Chang[13], Zhenzhong Zeng[9], Yongshuo Fu[8], Baolin Xue[14], Ping Wang[15], Kefei Zhao[16], Le Li[16], Wenkai Li[17], Yumei Li[18], Mi Jiang[19], Yuanhe Yang[20], Haihua Shen[20], Xia Zhao[20], Yue Shi[20], Bo Wu[20], Zhengbing Yan[20], Mengjia Wang[21], Yanjun Su[20], Tianyu Hu[20], Qin Ma[22,23,24], Hao Bai[2,3], Lijun Wang[25,2,3], Ziyan Yang[2,3,26], Yuhao Feng[2,3], Danhua Zhang[2,3], Erhan Huang[2,3], Jiamin Pan[2,3], Huiying Ye[2,3], Chen Yang[2,3], Yanwei Qin[2,3], Chenqi He[2,3], Yanpei Guo[2,3], Kai Cheng[27], Yu Ren[27], Haitao Yang[27], Chengyang Zheng[2,3], Jiangling Zhu[2,3], Shaopeng Wang[2,3], Chengjun Ji[2,3], Biao Zhu[2,3], Hongyan Liu[2,3], Zhiyao Tang[2,3], Zhiheng Wang[2,3], Shuqing Zhao[28], Yanhong Tang[2,3], Hanfa Xing[1], Qinghua Guo[27], Yu Liu[27], Jingyun Fang[2,3]

China's massive wave of urbanization may be threatened by land subsidence. Using a spaceborne synthetic aperture radar interferometry technique, we provided a systematic assessment of land subsidence in all of China's major cities from 2015 to 2022. Of the examined urban lands, 45% are subsiding faster than 3 millimeters per year, and 16% are subsiding faster than 10 millimeters per year, affecting 29 and 7% of the urban population, respectively. The subsidence appears to be associated with a range of factors such as groundwater withdrawal and the weight of buildings. By 2120, 22 to 26% of China's coastal lands will have a relative elevation lower than sea level, hosting 9 to 11% of the coastal population, because of the combined effect of city subsidence and sea-level rise. Our results underscore the necessity of enhancing protective measures to mitigate potential damages from subsidence.

As early as the 1920s, evidence of land subsidence was already detected in China's Shanghai and Tianjin cities (1–3). Nearly a century later, China is experiencing one of the most extensive urban expansions in human history (4). High-rise buildings are sprouting up, road systems are expanding, and groundwater is being used, all at a rapid pace. Although these activities have brought modern living for millions, they can also undermine the stability of urban land surface (5), potentially leading to widespread city subsidence. Instances of subsidence have been increasingly reported in major Chinese cities (1, 6–10). However, existing research differs in timeframe and methodologies, highlighting the absence of a systematic assessment at the national scale. As a result, the extent, pattern, and velocity of subsidence in China's cities remain unclear.

Also unclear is the size of China's urban population exposed to subsidence. As of 2020, China's urban areas were home to 920 million people (11), making it the largest urban population in the world. Even a small portion of subsiding land in China could therefore translate into a substantial threat to urban life. Subsidence leads to ground fissures, damages buildings and civil infrastructure, and increases the risk of floods, many of which can result in injuries or loss of lives. Over the past decades, subsidence-related disasters in China have already incurred an annual direct economic loss of more than 7.5 billion yuan, accompanied by hundreds of fatalities or injuries per year (12). The negative consequences of subsidence have been observed in both coastal and inland cities. However, coastal cities confront an additional risk from rising sea levels, which when combined with city subsidence can result in compound floods, posing serious threats to coastal population (13–16). Accurate mapping of city subsidence is crucial for guiding the implementation of sound measures to prevent or mitigate its consequences in both inland and coastal regions.

We provide a national-scale evaluation of China's city subsidence during 2015 to 2022, by leveraging the capability of the spaceborne Sentinel-1 Interferometric Synthetic Aperture Radar (InSAR) (17). Sentinel-1 InSAR offers a valuable tool with which to measure vertical land motions across extensive regions with a high spatial resolution (40 by 40 m in this study) (18–20). It complements the traditional Global Navigation Satellite System (GNSS) measurements (21), which are limited to point locations. Our study encompassed all Chinese cities with an urban population surpassing 2 million, all provincial capitals, and key industrial cities, totaling 82 major cities and including 74% of China's urban population (table S1) (22, 23). We used a standardized InSAR processing approach to produce internally consistent observations, which were further validated against GNSS ground measurements (22). We first quantified the severity of the city subsidence and uncovered its national pattern, with uncertainties in InSAR measurement accounted for. Subsequently, we associated the observed subsidence with various factors such as groundwater change and building weight (22). Next, we linked city subsidence to urban population to gain insight into the size of urban population that is affected by city subsidence. Last, we projected the coastal urban lands that could be inundated in the coming 100 years and the corresponding impact on coastal population, considering the combined effect of sea-level rise and city subsidence (22).

National pattern of city subsidence

We used three indicators to comprehensively assess the severity of land subsidence. The first indicator, denoted as P_{3mm}, measures the proportion of pixels (each pixel covering a land area of 40 by 40 m) that are subsiding with a velocity faster than 3 mm/year (or numerically <−3 mm/year). The selection of the 3 mm/year

[1]Beidou Research Institute, Faculty of Engineering, South China Normal University, Foshan 528000, China. [2]Institute of Ecology, College of Urban and Environmental Sciences, Peking University, Beijing 100871, China. [3]Key Laboratory for Earth Surface Processes of the Ministry of Education, Peking University, Beijing 100871, China. [4]College of Urban and Environmental Sciences, Peking University, Beijing 100871, China. [5]Department of Earth and Atmospheric Sciences, University of Houston, Houston, TX 77204, USA. [6]Department of Earth and Space Sciences, Southern University of Science and Technology, Shenzhen 518055, China. [7]River Basin Habitats Research Center, College of Architecture and Landscape Architecture, Peking University, Beijing 100871, China. [8]College of Water Sciences, Beijing Normal University, Beijing 100875, China. [9]School of Environmental Science and Engineering, Southern University of Science and Technology, Shenzhen 518055, China. [10]Earth Systems Research Center, Institute for the Study of Earth, Oceans, and Space, University of New Hampshire, Durham, NH 03824, USA. [11]Institute of Remote Sensing and Earth Sciences, Hangzhou Normal University, Hangzhou 311121, China. [12]Zhejiang Provincial Key Laboratory of Urban Wetlands and Regional Change, Hangzhou 311121, China. [13]College of Environmental and Resource Sciences, Zhejiang University, Hangzhou 310058, China. [14]Innovation Research Center of Satellite Application (IRCSA), Faculty of Geographical Science, Beijing Normal University, Beijing 100875, China. [15]Key Laboratory of Water Cycle and Related Land Surface Processes, Institute of Geographic Sciences and Natural Resources Research, Chinese Academy of Sciences, Beijing 100101, China. [16]School of Management, Guangdong University of Technology, Guangzhou 510520, China. [17]School of Geography and Planning, Sun Yat-sen University, Guangzhou 510006, China. [18]Institute of Zoology, Chinese Academy of Sciences, Beijing 100101, China. [19]School of Geospatial Engineering and Science, Sun Yat-sen University, Zhuhai 519082, China. [20]Institute of Botany, Chinese Academy of Sciences, Beijing 100093, China. [21]School of Geoscience and Technology, Zhengzhou University, Zhengzhou 450001, China. [22]School of Geographic Sciences, Nanjing Normal University, Nanjing 210023, China. [23]Key Laboratory of Virtual Geographic Environment (Nanjing Normal University), Ministry of Education, Nanjing, 210023, China. [24]Jiangsu Center for Collaborative Innovation in Geographical Information Resource Development and Application, Nanjing, 210023, China. [25]Faculty of Geosciences and Environmental Engineering, Southwest Jiaotong University, Chengdu 611756, China. [26]College of Forestry, Beijing Forestry University, Beijing 100083, China. [27]Institute of Remote Sensing and Geographic Information System, School of Earth and Space Sciences, Peking University, Beijing 100871, China. [28]School of Ecology, Hainan University, Haikou 570228, China.
*Corresponding author. Email: sltao@pku.edu.cn
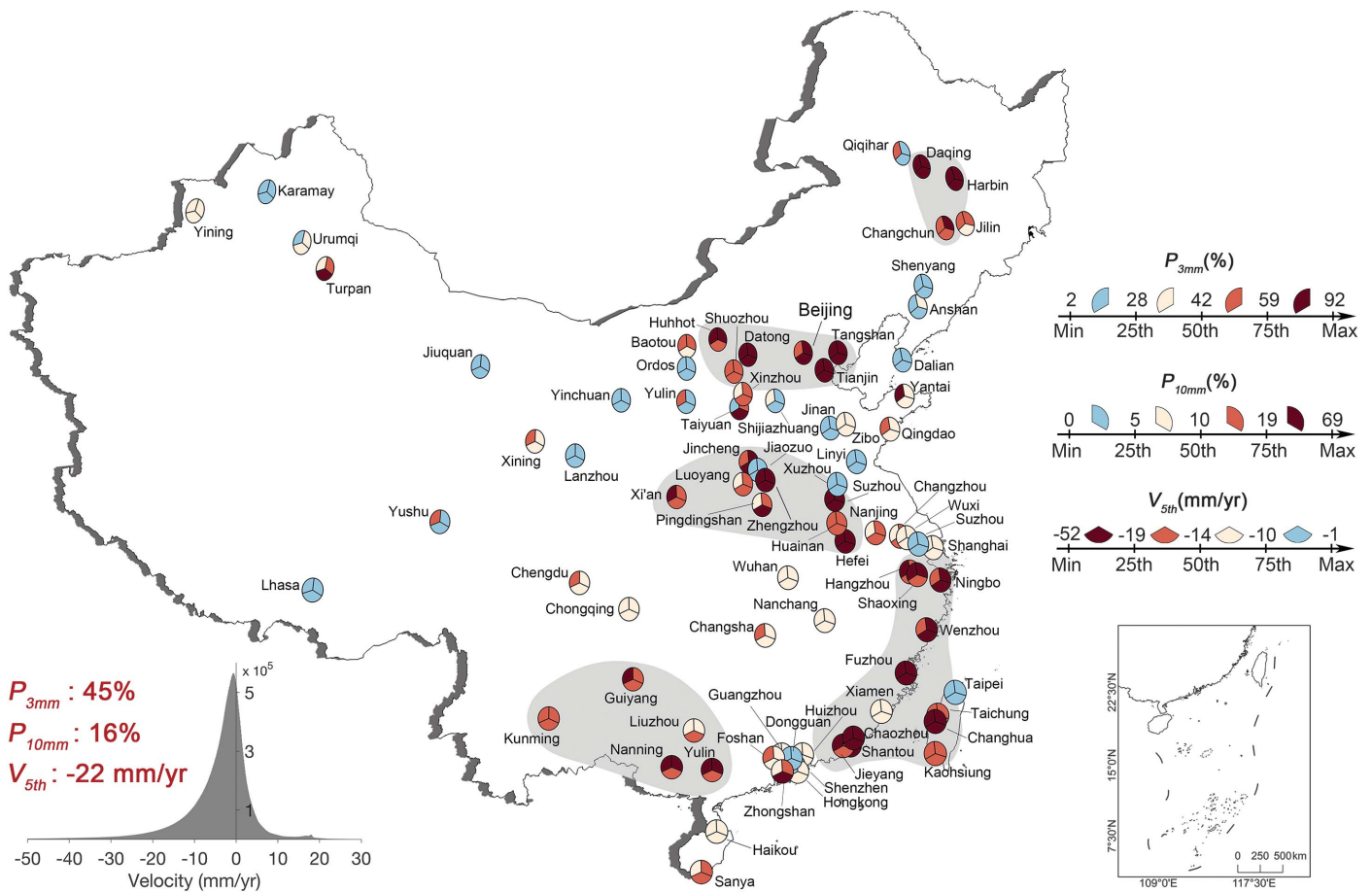†These authors contributed equally to this work.

Fig. 1. National pattern of city subsidence. Severity of city subsidence is indicated with three indicators: proportion of subsiding pixels faster than 3 mm/year (or numerically <−3 mm/year) (P_{3mm}, top left circular sector), proportion of subsiding pixels faster than 10 mm/year (or <−10 mm/year) (P_{10mm}, top right circular sector), and 5th percentile velocity of all pixels within a city (V_{5th}, bottom circular sector). Each pixel covers a land area of 40 by 40 m. The 3 mm/year threshold was used because GNSS validation revealed an uncertainty of 3 mm/year in InSAR-derived land subsidence (figs. S3 and S4). P_{3mm}, P_{10mm}, and V_{5th} values of the cities are divided into quartiles (four approximately equal parts) and colored differently. The gray shaded areas delineate five regions dominated by fast-subsiding cities. (**Inset**) The P_{3mm}, P_{10mm}, and V_{5th} values of all the pixels from all cities. More information on the cities can be found in table S1.

threshold was based on GNSS validation, which revealed an uncertainty of 3 mm/year in InSAR-derived land subsidence (22). Thus, P_{3mm} signifies the most realistic proportion of all subsiding lands after accounting for measurement uncertainty. The second indicator, referred to as P_{10mm}, is the proportion of pixels with a subsidence velocity faster than 10 mm/year (or <−10 mm/year). It complements P_{3mm} by providing additional insight into the extent of rapid subsidence in urban lands. The third indicator, denoted as V_{5th}, represents the 5th percentile velocity of all pixels. Median velocity was also examined, but the national pattern of subsidence shown below was not altered (fig. S1).

Our results based on the indicator of P_{3mm} revealed pervasive land subsidence in China's major cities. At the national scale, nearly half (44.7%) of all the pixels of the 82 cities are subsiding faster than 3 mm/year (or <−3 mm/year). P_{10mm} further revealed that 15.8% of the pixels are subsiding rapidly (<−10 mm/year). The value

V_{5th} was estimated to be −22 mm/year, suggesting that about 5% of the urban lands are subsiding faster than 22 mm/year (Fig. 1).

Further calculating the three indicators for each city (Fig. 1 and table S1), Changhua showed the largest values of P_{3mm} (92%) and P_{10mm} (69%), whereas Tianjin exhibited the lowest V_{5th} velocity (−52 mm/year). At a larger scale, the three indicators consistently suggested that cities facing severe subsidence (Fig. 1, red and dark red circles; fig. S2; and table S1) are concentrated in five regions (Fig. 1, shaded gray areas). Starting from northern to southern China, the first region is situated in northeastern China, anchored by cities that have served as China's industrial hubs since the 1950s, including Daqing (P_{3mm}, 62%; P_{10mm}, 26%; V_{5th}, −22 mm/year), Harbin (P_{3mm}, 65%; P_{10mm}, 26%; V_{5th}, −19 mm/year), and Changchun (P_{3mm}, 57%; P_{10mm}, 21%; V_{5th}, −19 mm/year). The second region is located in central-northern China, with Beijing (P_{3mm}, 47%; P_{10mm}, 30%; V_{5th}, −37 mm/year) and Tianjin (P_{3mm}, 90%; P_{10mm}, 66%; V_{5th}, −

52 mm/year) as typical examples. This region overlaps with China's capital zone, where population density and groundwater demand are extremely high (24). The third region is identified in central China, containing several renowned industrial cities such as Pingdingshan (P_{3mm}, 38%; P_{10mm}, 13%, V_{5th}, −28 mm/year), Jincheng (P_{3mm}, 55%; P_{10mm}, 20%; V_{5th}, −23 mm/year), and Huainan (P_{3mm}, 49%; P_{10mm}, 16%; V_{5th}, −17 mm/year). The fourth region is located in southern China and primarily includes provincial capital cities such as Kunming (P_{3mm}, 57%; P_{10mm}, 13%; V_{5th}, −15 mm/year), Nanning (P_{3mm}, 66%; P_{10mm}, 21%; V_{5th}, −18 mm/year), and Guiyang (P_{3mm}, 61%; P_{10mm}, 13%; V_{5th}, −14 mm/year). Last, in southeastern China, coastal cities such as Wenzhou (P_{3mm}, 50%; P_{10mm}, 24%; V_{5th}, −34 mm/year) and Shantou (P_{3mm}, 61%; P_{10mm}, 26%; V_{5th}, −21 mm/year) are subsiding rapidly, forming a coastal sinking belt.

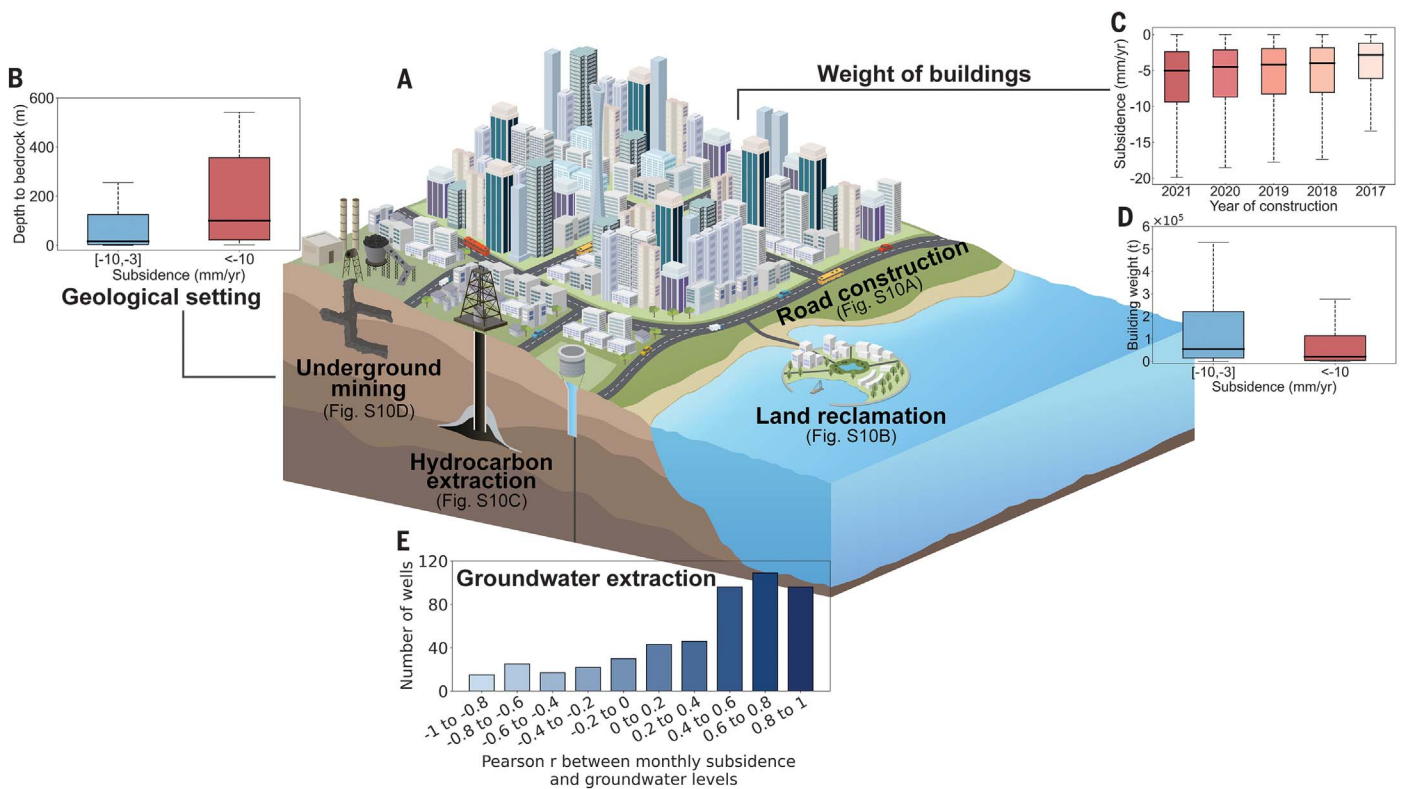The subsidence pattern we found does not resemble a large-scale land deformation pattern

Fig. 2. Associations between city subsidence and natural and human factors. (**A**) Schematic of the factors potentially contributing to city subsidence. (**B**) Depth to bedrock beneath moderately [(−10, −3) mm/year] and rapidly (<−10 mm/year) subsiding urban lands. (**C**) Variation in subsidence velocity across buildings constructed in different years. (**D**) Weight of buildings (in tonnes) in moderately [(−10, −3) mm/year] and rapidly (<−10 mm/year) subsiding urban lands. (**E**) Distribution of Pearson *r* values between monthly groundwater levels and monthly land subsidence. The significance levels and detailed examples on the temporal correlations are available in fig. S7. Instances of subsidence associated with construction of urban road system, coastal land reclamation, hydrocarbon extraction, and underground mining can be found in fig. S10.

(25). This highlights the critical need to focus specifically on urban areas and to analyze subsidence by using a consistent methodological framework. The results and pattern are unlikely to be affected by uncertainties of InSAR-derived velocity because 3 and 10 mm/year fall beyond the range of uncertainty in InSAR-derived velocity (figs. S3 to S5).

City subsidence linked to natural and human factors

In addition to the national pattern of city subsidence, we identified several natural and human factors that were associated with city subsidence (Fig. 2A) (26). The first factor is the geological setting beneath the city. We observed an obvious difference in depth to bedrock between moderately [(−10, −3) mm/year] and rapidly (<−10 mm/year) subsiding lands (Fig. 2B), highlighting the impact of geology on subsidence.

Closely related with the geological setting is the weight of buildings, which exerts geostatic pressure on the urban subsurface (27). The pressure can cause both elastic changes in the deeper bedrock and crust and inelastic consolidation of the shallower sediment. The former is usually small (27), whereas the latter can be

substantial, especially in the initial years after construction (28). We indeed observed such a phenomenon: The later the building is constructed, the faster the subsidence tends to be (Fig. 2C). We also found that heavier buildings tend to subside more slowly (Fig. 2D), possibly because they are anchored on deeper rock and are therefore less prone to subside (29). This hypothesis was supported by ground-recorded piling depth data from Shanghai (fig. S6).

Another major factor is groundwater loss, which decreases pore pressure and leads to subsurface compaction (5, 8). This has been observed worldwide such as in Houston, Mexico City, and Delhi of India (30–33) and is no exception in China. By compiling a database comprising 1619 groundwater monitoring wells (34), we observed quite widespread influence of groundwater changes on subsidence in China's cities: 65% of the Pearson correlation coefficient (*r*) values between monthly groundwater measurements and monthly subsidence exceeded 0.4, a value that corresponds approximately to a significance level of 0.01 (Fig. 2E and fig. S7). Most of the groundwater changes were anthropogenic, with only 12% exhibiting relatively high correlations with precipitation dy-

namics (Pearson *r* > 0.4) (fig. S8). In particular, some groundwater changes in northern China are the result of government efforts, such as the South-North Water Diversion Project, which transfers water from the Yangtze River to northern cities (35, 36). These efforts raised groundwater levels and stabilized city subsidence, as evidenced in Beijing (fig. S9).

Some factors exhibited effects that were not consistently observed across all cities (fig. S10). Urban transportation systems, for example, cause subsoil and track bed compaction through repeated dynamic loading and traffic vibration, potentially contributing to subsidence (2). Such is the case in mega cities such as Beijing, where regions around the subways and highways are sinking with a minimum speed of −45 mm/year (fig. S10A). Land reclamation has been carried out in several coastal cities in China, and reclaimed lands are vulnerable to subsidence owing to sedimentary consolidation (37). In Haikou, reclaimed lands have been subsiding with a minimum speed of −20 mm/year (fig. S10B). Land subsidence also occurs in hydrocarbon extraction areas experiencing a reduction of fluid pressure and consequent compaction of reservoir rocks. One of the earliest cases of
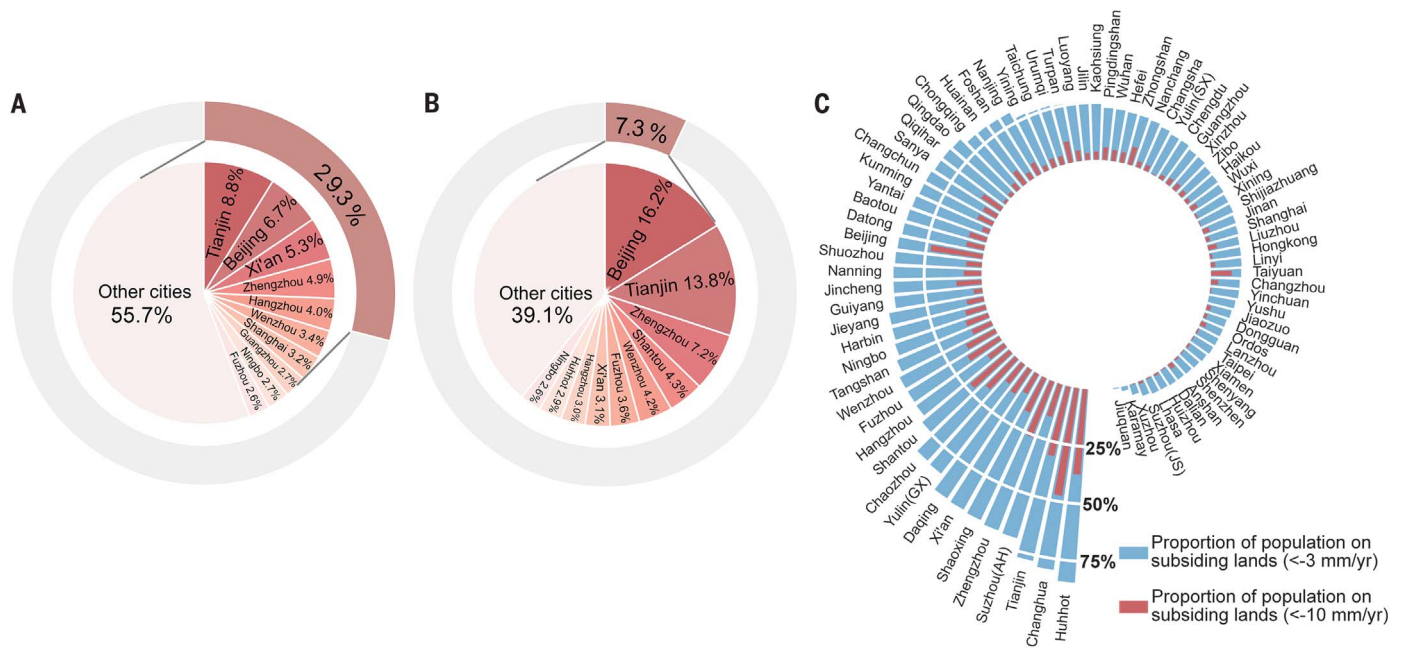
Fig. 3. Population living on subsiding urban lands. (**A**) Proportion of population living on urban lands subsiding faster than 3 mm/year (or <−3 mm/year) at the national level (outer circle) and top 10 cities with the largest population residing on these lands (inner circle). (**B**) Similar to (A), but showing the proportion of population living on urban lands subsiding faster than 10 mm/year (or <−10 mm/year). (**C**) City-specific proportion of population living on urban lands subsiding faster than 3 mm/year (blue) and that on urban lands subsiding faster than 10 mm/year (red).
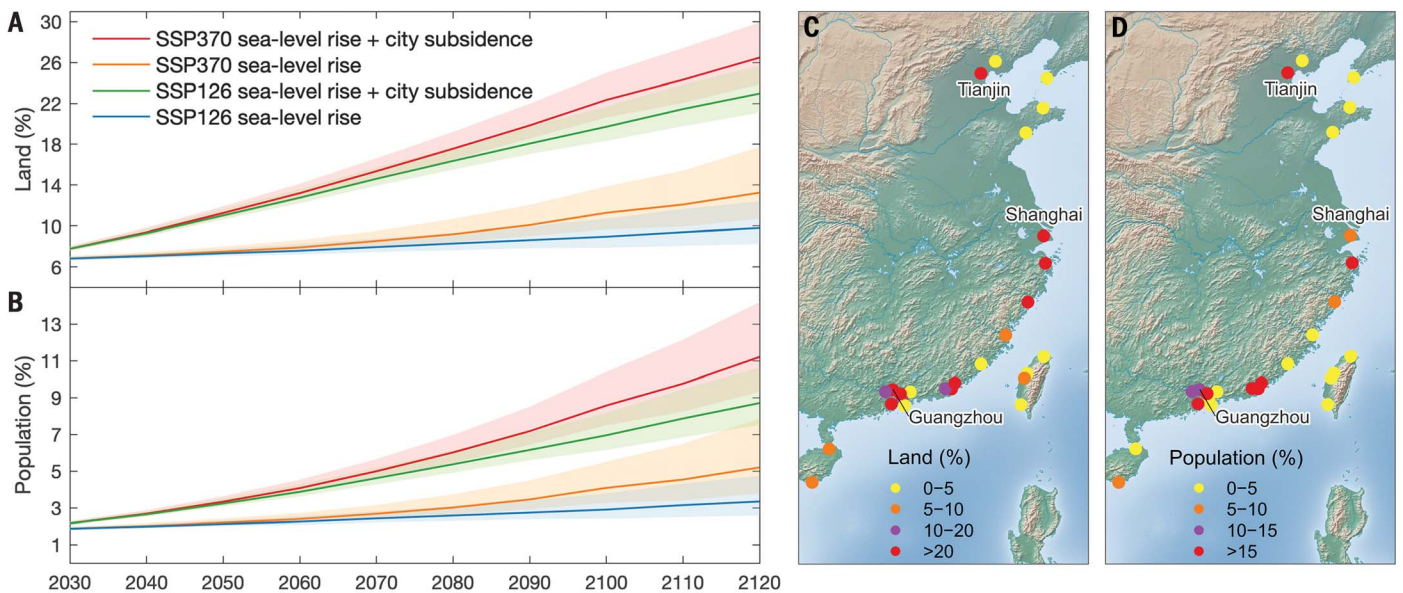
Fig. 4. Exposure of coastal lands and population to the combined effect of sea-level rise and city subsidence. (**A**) Proportion of urban lands that will have a relative elevation lower than sea level over the next 100 years across four different scenarios, considering all coastal cities collectively. The thick lines indicate estimations made with sea-level rise projections with median likelihood. The lightly shaded ranges indicate the estimations made with the 17th to 83rd percentile likely ranges (67% probability) of sea-level rise projections. (**B**) Proportion of population residing on urban lands that will have a relative elevation lower than sea level in the four different scenarios. (**C**) City-specific proportion of lands with a relative elevation lower than sea level in 2120 in the "worst-case" scenario (SSP 370 sea-level rise + city subsidence). (**D**) City-specific proportion of population living on urban lands with a relative elevation lower than sea level in 2120 in the "worst-case" scenario (SSP 370 sea-level rise + city subsidence). The base maps in (C) and (D) depict elevations.

hydrocarbon-induced subsidence was observed in the Goose Creek oil fields near Houston, Texas (*38*). In China's Daqing city (fig. S10C), subsidence up to −31 mm/year occurred around the oil field rather than directly within it, possibly because of the extraction of water from areas near the oil field and its subsequent injection into the oil field (*39*). Underground mining is also associated with subsidence because it creates empty spaces and often lowers the groundwater level (*40*). In the northern part of Pingdingshan, one of the largest coal bases of China (*41*), fast

land subsidence up to –109 mm/year is occurring (fig. S10D).

The aforementioned phenomena may occur concurrently in a given region, and separating their contributions requires the application of physical models or a combination of various methods (26). Planning of mitigation strategies will benefit from ongoing and future efforts to accurately identify physical causes of subsidence and link each driver to a specific human activity or natural phenomenon. Although currently these tasks remain challenging at a broad spatial scale, we propose that the key to addressing China's city subsidence could lie in the long-term, sustained control of groundwater extraction. As we have shown, the widespread impact of groundwater depletion on subsidence is evident (Fig. 2E), and the resulting subsidence rates are usually fast (12, 42). In a global context, long-term control of groundwater extraction has demonstrated success in stabilizing subsidence, as observed in Tokyo and Osaka, Japan, whereas short-term and incomplete control has proven ineffective, as exemplified in Queretaro, Mexico (30, 43, 44). Shanghai and its neighboring areas have been actively pursuing long-term control of groundwater extraction, which likely explains the slow subsidence observed there (45, 46).

Exposure of urban population to subsidence and sea-level rise

Last, to gain insight into the size of urban population that is affected by land subsidence, we linked China's city subsidence to urban population (22). About one-third (29.3%) of the population of the 82 cities resides in regions subsiding faster than 3 mm/year (Fig. 3A), and 7.3% live in regions subsiding faster than 10 mm/year (Fig. 3B). If the former percentage were applied to the total urban population of China, 270 million people would be living on sinking lands (faster than 3 mm/year), close to one-third of the population in Europe. If the percentage of 7.3% were applied, 67 million people would be living in rapidly sinking regions (faster than 10 mm/year), roughly equaling the population of France.

Of the 82 cities, 10 accounted for nearly or more than half of the entire population residing in subsiding regions. For example, concerning the population living in regions subsiding faster than 3 mm/year, Tianjin and Beijing contributed 8.8 and 6.7%, respectively. For the population living in regions subsiding faster than 10 mm/year, these two cities accounted for as much as 13.8 and 16.2%, respectively. We also examined, for each of the 82 cities, the proportion of population living on subsiding lands (Fig. 3C). The 10 cities generally had high percentages, although not the highest. Huhhot had the highest percentage (84%) of population living in regions subsiding faster than 3 mm/year, whereas Changhua had the highest percentage

(47%) of population living in regions subsiding faster than 10 mm/year (Fig. 3C).

In coastal regions, land subsidence can amplify the risk of inundation caused by rising sea levels (47). We therefore also projected the proportion of coastal lands that will have a relative elevation lower than sea level under the combined effect of sea-level rise and land subsidence by 2120 (22). Toward this end, velocity of city subsidence was assumed as constant over the next 100 years, with uncertainty evaluated and controlled (fig. S11) (22). Sea-level rise projections were obtained from the Intergovernmental Panel on Climate Change (IPCC) under Shared Socioeconomic Pathway (SSP) 126 and SSP 370 scenarios (48, 49). The SSP 585 scenario was not considered in light of the recent argument asserting its high improbability (50). To mitigate the impact of elevation uncertainty on the projection, median elevation values across nine products were calculated on a per-pixel basis (22).

We found that the land area with a relative elevation lower than sea level was projected to increase by 2.7 to 3.3 times in 2120 compared with 2020 (Fig. 4A), indicating the potential for widespread inundation unless well protected. In 2020, the proportion of land with a relative elevation below sea level was ~6%. However, in the scenario of "SSP 126 sea-level rise + city subsidence," this proportion will increase to 22% in 2120, whereas in the "SSP 370 sea-level rise + city subsidence" scenario it will reach 26% (Fig. 4A). Similarly, the proportion of affected coastal population was projected to largely increase from 2% in 2020 to 9% in 2120 in the "SSP 126 sea-level rise + land subsidence" scenario, and from 2 to 11% in the "SSP 370 sea-level rise + city subsidence" scenario (Fig. 4B). This increase can be primarily attributed to city subsidence rather than sea-level rise. For example, the difference in land area with a relative elevation lower than sea level between SSP126 and SSP370 sea-level rise scenarios will be 5% in 2120. However, the difference between "SSP126 sea-level rise" and "SSP126 sea-level rise + city subsidence" scenarios will be ~13%. This suggests that neglecting land subsidence would result in a substantial underestimation of the potential area and population that could be inundated. Further focusing on the worst-case scenario ("SSP 370 sea-level rise + city subsidence") at the individual city level, Tianjin, Shanghai, and the city cluster around Guangzhou showed the most exposures (Fig. 4, C and D, and figs. S12 and S13).

We emphasize that the above analysis only involved changes in elevation relative to sea level and did not account for the effect of coastal dike systems, primarily because of the lack of a high-resolution map depicting the distribution of dikes. Hence, the result is an estimate of coastal lands and population that could face inundation if not adequately protected. This

underscores the crucial role of coastal dike systems in preventing inundation. Compared with the losses incurred from flooding, coastal dikes have been demonstrated as a cost-efficient means for flood prevention (fig. S14). China has established a tremendous dike system (15). However, dikes themselves are also prone to subside (51). Ensuring their effectiveness through constant maintenance and improvement is crucial for reducing the risk of coastal inundation.

Conclusions

We provided a national-scale, systematic evaluation of China's city subsidence. Of the urban lands in China's major cities, 45% are subsiding with a velocity faster than 3 mm/year, and 16% are subsiding faster than 10 mm/year; these urban lands contain 29 and 7% of urban population, respectively. We also projected the proportion of coastal lands that will have a relative elevation lower than sea level, and the corresponding impact on coastal population, because of the combined effects of city subsidence and sea-level rise over the next 100 years (16). We found a considerable risk of coastal inundation unless adequate protective measures are implemented and maintained. China has been actively taking a range of measures to mitigate city subsidence (46), such as control of groundwater extraction and interbasin water transfers (35, 36, 46, 52). In this context, we provide comprehensive maps of city subsidence across China, aiding in the precise identification of sinking regions and the formulation of mitigation measures. Effectively addressing the challenge of city subsidence ultimately demands collaborative and coordinated endeavors from stakeholders across various tiers, including policy-makers, the research community, and civil engineers.

REFERENCES AND NOTES

1. R. L. Hu, Z. Q. Yue, L. C. Wang, S. J. Wang, *Eng. Geol.* **76**, 65–77 (2004).
2. Y. S. Xu, L. Ma, Y. J. Du, S. L. Shen, *Nat. Hazards* **63**, 1255–1267 (2012).
3. W. Tang, W. Zhan, B. Jin, M. Motagh, Y. Xu, *IEEE J. Sel. Top. Appl. Earth Obs. Remote Sens.* **14**, 2621–2633 (2021).
4. K. C. Seto, M. Fragkias, B. Güneralp, M. K. Reilly, *PLOS ONE* **6**, e23777 (2011).
5. G. Herrera-García *et al.*, *Science* **371**, 34–36 (2021).
6. Y. Q. Xue, Y. Zhang, S.-J. Ye, J.-C. Wu, Q.-F. Li, *Environ. Geol. (Berl.)* **48**, 713–720 (2005).
7. MLR (Ministry of Land and Resources), MWR (Ministry of Water Resources), "The prevention and control planning of land subsidence in China (2011–2020)" (Ministry of Water Resources, 2012); https://www.gov.cn/gzdt/2012-07/06/content_2178070.htm (In Chinese).
8. M. Bagheri-Gavkosh *et al.*, *Sci. Total Environ.* **778**, 146193 (2021).
9. X. Shi *et al.*, *Nat. Hazards Earth Syst. Sci.* **21**, 2285–2297 (2021).
10. J. Dong *et al.*, *Remote Sens. Environ.* **286**, 113446 (2023).
11. National Bureau of Statistics of P. R. China, *China Statistical Yearbook* (China Statistics Press, 2021) (In Chinese).
12. China Meteorological Administration (CMA), *Ground Subsidence: The Pain of Cities* (CMA, 2014); https://www.cma.gov.cn/2011xzt/2014zt/20140508/2014050805/201405/t20140512_245869.html (In Chinese).

13. M. E. Hauer, J. M. Evans, D. R. Mishra, *Nat. Clim. Chang.* **6**, 691–695 (2016).
14. M. Shirzaei *et al.*, *Nat. Rev. Earth Environ.* **2**, 40–58 (2021).
15. J. Fang *et al.*, *Nat. Commun.* **13**, 6946 (2022).
16. R. J. Nicholls *et al.*, *Nat. Clim. Chang.* **11**, 338–342 (2021).
17. D. Massonnet, K. L. Feigl, *Rev. Geophys.* **36**, 441–500 (1998).
18. E. Blackwell, M. Shirzaei, C. Ojha, S. Werth, *Sci. Adv.* **6**, eaba4551 (2020).
19. C. Tay *et al.*, *Nat. Sustain.* **5**, 1049–1057 (2022).
20. P. C. Wu, M. Wei, S. D'Hondt, *Geophys. Res. Lett.* **49**, e2022GL098477 (2022).
21. G. Wang, A. Greuter, C. M. Petersen, M. J. Turco, *J. Surv. Eng.* **148**, 04022008 (2022).
22. Materials and methods are available as supplementary materials.
23. National Bureau of Statistics, *Bulletin of the Seventh National Population Census* (China Statistics Press, 2021) (In Chinese).
24. W. Feng *et al.*, *Water Resour. Res.* **49**, 2110–2118 (2013).
25. X. Chen *et al.*, *Seismol. Geomagn. Observ. Res.* **42**, 183–190 (2021) (In Chinese).
26. T. Candela, K. Koster, *Science* **376**, 1381–1382 (2022).
27. T. Parsons, *AGU Adv.* **2**, e2020AV000277 (2021).
28. Z. D. Cui, J. Q. Yang, L. Yuan, *Nat. Hazards* **79**, 1199–1217 (2015).
29. M. Korff, R. J. Mair, F. A. F. Van Tol, *J. Geotech. Geoenviron. Eng.* **142**, 04016034 (2016).
30. P. Castellazzi, J. Garfias, R. Martel, *Int. J. Appl. Earth Obs. Geoinf.* **105**, 102632 (2021).
31. E. Chaussard, E. Havazli, H. Fattahi, E. Cabral-Cano, D. Solano-Rojas, *J. Geophys. Res. Solid Earth* **126**, e2020JB020648 (2021).
32. S. Garg, M. Motagh, J. Indu, V. Karanam, *Sci. Rep.* **12**, 651 (2022).
33. M. F. Hasan, R. Smith, S. Vajedian, R. Pommerenke, S. Majumdar, *Nat. Commun.* **14**, 6180 (2023).
34. Z. Ao *et al.*, Monthly groundwater data in China (2018-2021). figshare (2024); https://doi.org/10.6084/m9.figshare.24942165.
35. D. Long *et al.*, *Nat. Commun.* **11**, 3665 (2020).
36. X. Yu, G. Wang, X. Hu, Y. Liu, Y. Bao, *Remote Sens. (Basel)* **15**, 1647 (2023).
37. S.-W. Park, S.-H. Hong, *Geophys. Res. Lett.* **48**, e2020GL090970 (2021).
38. T. L. Holzer, R. L. Bluntzer, *Ground Water* **22**, 450–459 (1984).
39. B. Hu, H. Li, X. Zhang, L. Fang, *IEEE Geosci. Remote Sens. Mag.* **8**, 108–134 (2020).
40. A. Behera, K. S. Rawat, *Mater. Today Proc.* (2023).
41. C. Zhai, X. Xiang, J. Xu, S. Wu, *Nat. Hazards* **82**, 507–530 (2016).
42. Y. Xu, S. Shen, Z. Cai, G. Zhou, *Nat. Hazards* **45**, 123–135 (2008).
43. S. Kaneko, T. Toyota, in *Groundwater and Subsurface Environments: Human Impacts in Asian Coastal Cities*, M. Taniguchi, Ed. (Springer, 2011), pp. 249–270.
44. A. Cao *et al.*, *Curr. Opin. Environ. Sustain.* **50**, 87–97 (2021).
45. X. Shi *et al.*, *Environ. Earth Sci.* **75**, 195 (2016).
46. S. Ye, Y. Xue, J. Wu, X. Yan, J. Yu, *Hydrogeol. J.* **24**, 685–693 (2016).
47. J. C. L. Normand, E. Heggy, P. Castellazzi, *IEEE J. Sel. Top. Appl. Earth Obs. Remote Sens.* **16**, 9286–9301 (2023).
48. B. Fox-Kemper *et al.*, in *Climate Change 2021—The Physical Science Basis: Working Group I Contribution to the Sixth Assessment Report of the Intergovernmental Panel on Climate Change* (Cambridge Univ. Press, 2023), pp. 1211–1362.
49. G. G. Garner *et al.*, IPCC AR6 Sea Level Projections, version 20210809. Zenodo (2024); https://doi.org/10.5281/zenodo.6382554.
50. Z. Hausfather, G. P. Peters, *Nature* **577**, 618–620 (2020).
51. J. Yin *et al.*, *J. Hydrol.* **571**, 593–604 (2019).
52. The State Council of the People's Republic of China, "Regulation on Groundwater Management" (The State Council of the People's Republic of China, 2021); https://www.gov.cn/zhengce/content/2021-11/09/content_5649924.htm (In Chinese).

SUPPLEMENTARY MATERIALS